Electronic Supplementary Material (ESI) for Physical Chemistry Chemical Physics.

Supporting Information

Temperature dependence of cross-effect dynamic nuclear polarization in rotating solids: advantages of elevated temperatures

Michel-Andreas Geiger[a][+], Marcella Orwick-Rydmark[a][+], Katharina Märker[a], W. Trent Franks[a], Dmitry Akhmetzyanov[b], Daniel Stöppler[a], Maximilian Zinke[a], Edgar Specker[a], Marc Nazaré[a], Anne Diehl[a], Barth-Jan van Rossum[a], Fabien Aussenac[c], Thomas Prisner[b], Ümit Akbey[a], and Hartmut Oschkinat*[a]

Supporting information

Table of contents

1. Radical synthesis

1.1 General Information

Chemicals and solvents were obtained from commercial sources and used without further purification. Reactions that required dry conditions were conducted under a nitrogen atmosphere using standard Schlenk techniques and commercially available anhydrous solvents stored over molecular sieves. Column chromatography for the purification of reaction mixtures was performed on a CombiFlash Rf 200 (Teledyne Isco) that was equipped with a binary pump and an automated fraction collector, triggered by a UV detector. RediSep Rf Normal-phase Silica Flash Columns were used for the separations.

Reaction controls were performed on an Agilent 1260 LC-MS system equipped with a diode array detector and a single quadrupole mass spectrometer (Agilent 6120). High-resolution ESI-TOF mass spectra for structure verification were obtained from an Agilent 1200 LC-MS system equipped with a diode array detector and an accurate-mass time-of-flight mass spectrometer (Agilent G6220A). Mixtures of water and acetonitrile with 0.1 % formic acid were used as eluents in both LC-MS systems. Samples were dissolved in MeCN/H_2O 1:1. Routine solution NMR spectra (^{1}H, ^{13}C) were recorded on a Bruker AV300 spectrometer in $CDCl_3$. Chemical shifts are reported in ppm relative to the residual solvent peak.[1]

1.2 Synthetic concept

The synthesis of deuterated TOTAPOL radicals was done following known procedures from literature, using deuterated 4-amino-TEMPO (5) and 4-hydroxy-TEMPO (4) as main building blocks[2] (see SI-Scheme (1)). For their preparation, deuterated 4-oxo-tetramethylpiperidine (2) was synthesized from deuterated acetone and ammonium chloride and further reacted with hydrogen peroxide in the presence of sodium tungstate to yield the nitroxide radical (3)[3,4]. The deuterium content in the methylene groups was then adjusted by equilibration in H_2O/D_2O at the desired deuterium (D_2O) concentration[5]. The resulting ketone was further reacted with 4-hydroxy-TEMPO (4) and 4-amino-TEMPO (5), using $NaBH_4$ or $NaBH_3CN$ and ammonium acetate, respectively[6, 7]. TOTAPOL (1) was then synthesized according to the standard procedure[2], by first reacting 4-hydroxy-TEMPO (4) with epichlorohydrine and then linking the two nitroxides 4-(2,3-epoxypropoxy)-TEMPO (6) and 4-amino-TEMPO (5) in the last step.

By utilizing the presence of exchangeable protons/deuterons in the radical precursors, this synthetic route represents a cost-efficient alternative to the exclusive use of deuterated solvents and reagents, which is often reported in literature[8]. Moreover, it provides a simple method to control the degree of deuteration in the CH_2 groups.

Detailed descriptions of all reactions are given in the following sections. Synthetic intermediates are named according to the convention introduced in this paper, indicating the percentage of deuterium in 3- and 5-positions as a number behind the name of the molecule.

1.3 Synthetic route to CD_3-TOTAPOL-X isotopologues

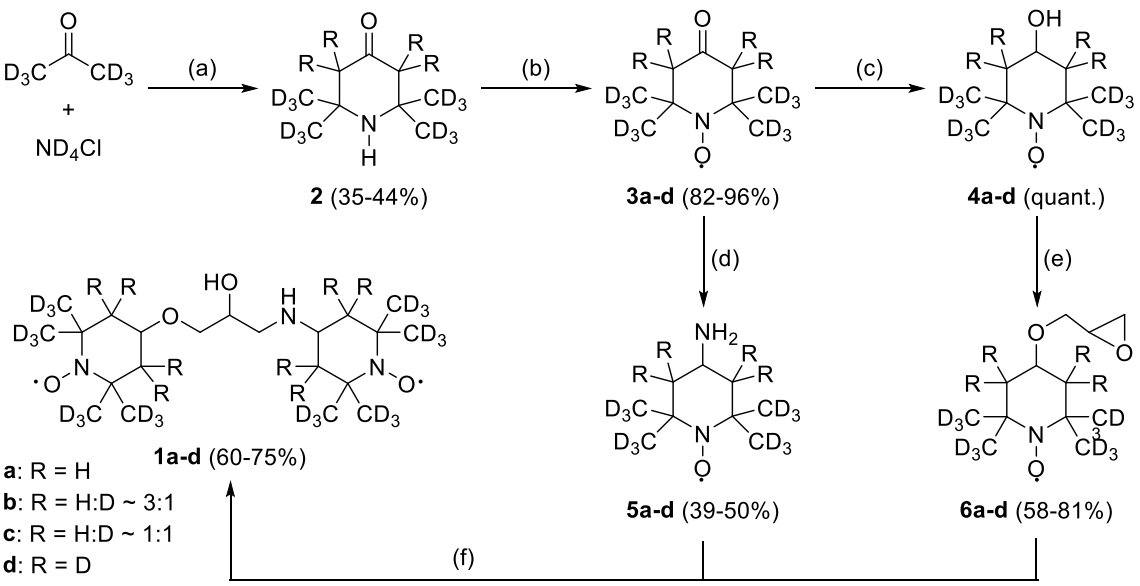

SI-Scheme 1: Synthetic route to deuterated TOTAPOL isotopologues. Reagents and reaction conditions: (a) Na_2CO_3, MgO, 50°C, 3 d. (b) 1. H_2O_2, Na_2WO_4, Na_4EDTA, 23°C, 12 h. 2. Na_2CO_3/D_2O, 23°C, 12 h. (c) $NaBH_4$, 0 °C, 1 h. (d) NH_4OAc/ND_4OAc, $NaBH_3CN$, 23 °C, 2 h. (e) epichlorhydrin, 23°C, 2 d. (f) $LiClO_4$, 40°C, 3 d.

1.4 Experimental procedures

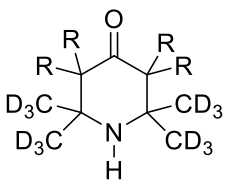

2

SI-Figure 1: structure of 4-oxo-2,2,6,6-tetramethylpiperidine (2)

A suspension of ND_4Cl (1 eq.), anhydrous Na_2CO_3 (0.5 eq.) and MgO (1.25 eq.) in D_6-acetone (3-4 eq.) was stirred at 50° C for 3 days. It was then cooled to RT, diluted with acetone and filtered. The filter cake was pulverized and washed again with acetone. The combined filtrates were concentrated in vacuum and purified by column chromatography (DCM → DCM/MeOH 95:5). The product was obtained as yellow-orange needles (35 - 44 %) and used as such in the next step. No adjustment of H/D content in 3- and 5-positions was performed at this level of the synthesis.

Representative analytical data for 4-oxo-2,2,6,6-tetramethylpiperidine-0 (2) (after D/H-exchange as described in the next step):

^{1}H-NMR (300 MHz, $CDCl_3$): δ = 2.22 (s, 2 x CH_2) ppm.

^{13}C-NMR (75 MHz, $CDCl_3$): δ = 211.06 (CO), 55.20 ($C(CD_3)_2$), 54.12 (CH_2), 31.02 (sept, J = 19.2 Hz, CD_3).

HR-MS (ESI-TOF): calcd for $C_9H_5D_{12}NO$ $[M + H]^+$ 168.2136, found 168.2131.

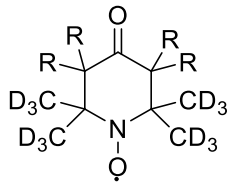

3a-d

a: R = H
b: R = H:D ~ 3:1
c: R = H:D ~ 1:1
d: R = D

SI-Figure 2: Structure of 4-oxo-2,2,6,6-tetramethylpiperidin-1-oxyl (3a-d)

H_2O_2 (35 wt% in H_2O, 2 eq.) was added drop wise to a solution of 4-oxo-2,2,6,6-tetramethylpiperidine (2, 1 eq.), Na_2WO_4 x 2 H_2O (10% wt) and Na_4EDTA x 2 H_2O (10 wt%) in H_2O (~1 ml/100 mg substance) that was continuously cooled on ice. The reaction mixture was stirred overnight at RT, basified with Na_2CO_3, and extracted with Et_2O. The combined organic layers were dried over Na_2SO_4 and the solvent was removed under reduced pressure. To adjust the H/D content in 3- and 5-positions of the resulting product to the desired 0/25/50/100 % level of deuterium, the substance was stirred overnight in a 0.4 M solution of anhydrous Na_2CO_3 in a H_2O/D_2O mixture (~ 1 ml per 100 mg substance) of the respective composition (100:0/75:25/50:50/0:100). The solution was extracted with diethyl ether, the combined organic layers were dried over Na_2SO_4 and the solvent was removed under reduced pressure. The product was obtained as orange-red needles (82 - 96 %) and used without further purification.

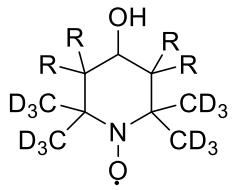

a: R = H
b: R = H:D ~ 3:1
c: R = H:D ~ 1:1
d: R = D

4a-d

SI-Figure 3: Structure of 4-hydroxy-2,2,6,6-tetramethylpiperidin-1-oxyl (4a-d)

A solution of 4-oxo-TEMPO (3a-d, 1 eq.) in the respective mixture of H_2O and D_2O (100:0/75:25/50:50/0:100 for a-d, 1-2 ml) was added drop wise to a solution of $NaBH_4$ (3 eq.) in the same mixture of H_2O and D_2O (2 ml) continuously cooled on ice. The reaction mixture was stirred for 5 minutes before it was warmed to RT, and subsequently stirred for one hour. The solution was diluted with brine (15 ml) and extracted with Et_2O. The combined organic fractions were dried over Na_2SO_4 and the solvent was evaporated under reduced pressure. The product was obtained as an orange-red solid and used without further purification.

4-Hydroxy-TEMPO-0 (4a): HR-MS (ESI-TOF): calcd for $C_9H_6D_{12}NO_2$ $[M + H]^+$ 185.2164, found 185.2154.

4-Hydroxy-TEMPO-25 (4b): HR-MS (ESI-TOF): calcd for $C_9H_5D_{13}NO_2$ $[M + H]^+$ 186.2226, found 186.2226.

4-Hydroxy-TEMPO-50 (4c): HR-MS (ESI-TOF): calcd for $C_9H_4D_{14}NO_2$ $[M + H]^+$ 187.2288, found 187.2289.

4-Hydroxy-TEMPO-100 (4d): HR-MS (ESI-TOF): calcd for $C_9H_2D_{16}NO_2$ $[M + H]^+$ 189.2415, found 189.2402.

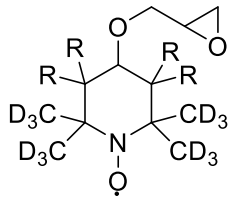

a: R = H
b: R = H:D ~ 3:1
c: R = H:D ~ 1:1
d: R = D

6a-d

SI-Figure 4: Structure of 4-(2,3-epoxypropoxy)-2,2,6,6-tetramethylpiperidin-1-oxyl(4-(2,3-epoxyprop-oxy)

4-Hydroxy-TEMPO (4a-d, 1 eq.) was added in portions to a solution of epichlorohydrin (5 eq.) and Bu_4NHSO_4 (0.04 eq.) in 50 % w/w aqueous NaOH (~

1 ml/100 mg substance) and stirred vigorously for 1-2 days at RT. The solution was poured onto ice and extracted with EtOAc. The combined organic layers were washed with brine, dried over Na_2SO_4, and the solvent was removed under reduced pressure. Purification by column chromatography (cyclohexane → cyclohexane/EtOAc 4:1) gave the product as a red solid (58 - 81 %).

4-(2,3-Epoxypropoxy)-TEMPO-0 (6a): HR-MS (ESI-TOF): calcd for $C_{12}H_{10}D_{12}NO_3$ $[M + H]^+$ 241.2426, found 241.2423.
4-(2,3-Epoxypropoxy)-TEMPO-25 (6b): HR-MS (ESI-TOF): calcd for $C_{12}H_9D_{13}NO_3$ $[M + H]^+$ 242.2488, found 242.2484.
4-(2,3-Epoxypropoxy)-TEMPO-50 (6c): HR-MS (ESI-TOF): calcd for $C_{12}H_8D_{14}NO_3$ $[M + H]^+$ 243.2551, found 243.2550.
4-(2,3-Epoxypropoxy)-TEMPO-100 (6d): HR-MS (ESI-TOF): calcd for $C_{12}H_6D_{16}NO_3$ $[M + H]^+$ 245.2677, found 245.2668.

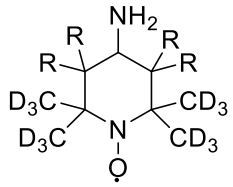

a: R = H
b: R = H:D ~ 3:1
c: R = H:D ~ 1:1
d: R = D

5a-d

SI-Figure 5: Structure of 4-amino-2,2,6,6-tetramethylpiperidin-1-oxyl (4-amino-TEMPO, 5a-d)

Deuterated ammonium acetate (ND_4OAc) was obtained by stirring NH_4OAc in MeOD (~1 ml/400 mg substance) for 2 h. The solvent was removed under reduced pressure until a white solid precipitated. The precipitant was dissolved in the same volume of MeOD, and the procedure was repeated 3X. Following the final resolubilization, the salt was thoroughly washed with Et_2O, collected by filtration, and dried under reduced pressure for 5 minutes. The product was directly used for the synthesis of 4-amino-TEMPO.

A mixture of anhydrous MeOH and MeOD (100:0/75:25/50:50/0:100 for a-d, respectively, 8 ml) was stirred over molecular sieves (3 Å) for one hour under dry conditions. A mixture of NH_4OAc and ND_4OAc (100:0/75:25/50:50/0:100 for a-d, respectively, 10 eq.) and a solution of 4-oxo-TEMPO (3a-d, 1 eq.) in the same

mixture of MeOH and MeOD (2 ml) were added. After the solution was stirred for one hour, $NaBH_3CN$ (1.4 eq.) was added in one portion and the reaction mixture was stirred for 16 h at RT. It was then filtered and the solvent was removed under reduced pressure. The remaining orange oil was taken up with water and DCM (1:1), filtered again, and the pH adjusted to ~ 5-6 with 2 M aqueous HCl. The aqueous layer was washed with DCM, its pH was raised to 13 by the addition of 2 M aqueous NaOH, and extracted with DCM. The organic layer was dried over Na_2SO_4, and the solvent was evaporated under reduced pressure. The remaining red oil was purified by column chromatography (DCM → DCM/MeOH 9:1) to give the product as a red solid (39 - 50 %).

4-Amino-TEMPO-0 (5a): HR-MS (ESI-TOF): calcd for $C_9H_7D_{12}N_2O$ $[M + H]^+$ 184.2323, found 184.2318.

4-Amino-TEMPO-25 (5b): HR-MS (ESI-TOF): calcd for $C_9H_6D_{13}N_2O$ $[M + H]^+$ 185.2386, found 185.2383.

4-Amino-TEMPO-50 (5c): HR-MS (ESI-TOF): calcd for $C_9H_5D_{14}N_2O$ $[M + H]^+$ 186.2449, found 186.2447.

4-Amino-TEMPO-100 (5d): HR-MS (ESI-TOF): calcd for $C_9H_3D_{16}N_2O$ $[M + H]^+$ 188.2574, found 188.2566.

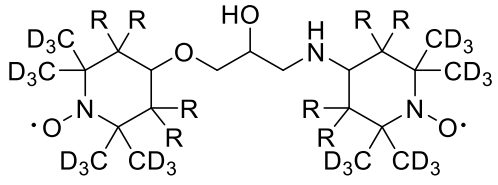

1a-d

a: R = H
b: R = H:D ~ 3:1
c: R = H:D ~ 1:1
d: R = D

SI-Figure 6: Structure of 1-(2,2,6,6-tetramethyl-1-oxy-4-piperidinyl)oxy-3-(2,2,6,6-tetramethyl-1-oxy-4-piperidinyl)amino-propan-2-ol (CD3-TOTAPOL, 1a-d)

Under dry conditions, a solution of 4-amino-TEMPO (5a-d, 1 eq.) in anhydrous MeCN (1-2 ml) was added to a solution of 4-(2,3-epoxypropoxy)-TEMPO (6a-d, 1 eq.) and $LiClO_4$ (1-2 eq. with respect to 4-(2,3-epoxypropoxy)-TEMPO) in anhydrous MeCN (2 ml). The reaction mixture was stirred for 3 to 4 days at 40 °C. The solvent was evaporated under reduced pressure and the crude product was purified by column

chromatography (DCM → DCM/MeOH 95:5) to yield TOTAPOL as an orange-red solid (60 - 75 %).

TOTAPOL-0 (1a): HR-MS (ESI-TOF): calcd for $C_{21}H_{17}D_{24}N_3O_4$ $[M + H]^+$ 424.4676, found 424.4677.

TOTAPOL-25 (1b): HR-MS (ESI-TOF): calcd for $C_{21}H_{15}D_{26}N_3O_4$ $[M + H]^+$ 426.4802, found 426.4785.

TOTAPOL-50 (1c): HR-MS (ESI-TOF): calcd for $C_{21}H_{13}D_{28}N_3O_4$ $[M + H]^+$ 428.4927, found 428.4932.

TOTAPOL-100 (1d): HR-MS (ESI-TOF): calcd for $C_{21}H_9D_{32}N_3O_4$ $[M + H]^+$ 432.5178, found 432.5175.

2 DNP Measurements

2.1 Sample preparation

Radicals were tested by means of two types of standard samples. For a first evaluation, uniformly ^{13}C, ^{15}N labelled proline (0.25-0.27 mM) was dissolved in GDH containing either 20 mM or 10 mM radical. As a more representative biological case, standard samples of crystalline uniformly ^{2}H, ^{15}N, ^{13}C SH3 preparations with 80 % ^{1}H back exchange were prepared in GDH with the different radicals (SI-Figure-7). The crystallinity of the SH3 samples in the presence of [D_8]-glycerol was monitored by synchrotron X-ray radiation. Crystals were found to be stable, allowing us to compare reproducible microcrystalline SH3 samples in the presence of the different radicals.

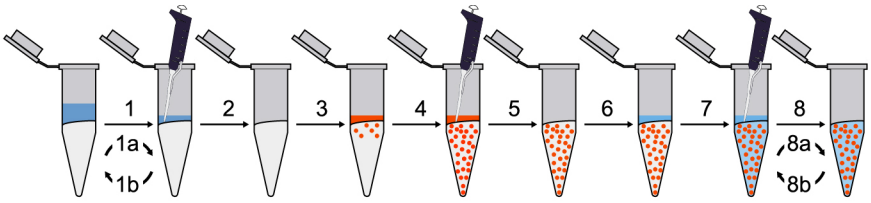

SI-Figure 7: Protocol for the preparation of SH3 DNP ssNMR samples containing 5-7 mg (m_{SH3}) DCN-labelled microcrystalline SH3

After initial precipitation in H_2O:D_2O (80%:20) the crystals were spun down by centrifugation (14.000 g; 4°C) (1a) to remove excess buffer (1b) that contained also protein (m_{SH3rem}). This step was repeated 2-3 times to obtain a wet-pellet m_{wp} (2). The weight of the wet pellet is determined, and water content calculated by subtracting the protein detected in the removed buffer from the total amount m_{SH3}, i.e. m_{SH3} - m_{SH3rem}. Afterwards a radical stock solution prepared in the removed buffer was added (3). After overnight incubation (4), excess liquid was removed (5). Water content was determined again as above. To achieve a final 60 % volume ratio of glycerol with respect to the remaining water (v/v), an appropriate amount of [D_8]-glycerol was added (6) taking the total water content into account. After 12 h of equilibration (7) excess buffer was removed again by cycles of centrifugation and pipetting (8a and 8b).

The conservation of the crystalline structure was further verified during DNP measurements via ^{13}C-^{13}C correlation spectroscopy in GDH at room temperature (SI Fig. 8, blue-green cross peaks), and confirmed by comparing the chemical shifts associated with the cross peaks of the amino acids alanine, isoleucine, threonine and valine to those observed in a solution spectrum (green) and in a solid-state ^{13}C-^{13}C correlation of microcrystalline material prepared without glycerol (red). For comparison, the spectra are plotted over a DNP enhanced ssNMR spectrum (blue) of the microcrystalline material in GDH that was prepared according to the procedure outlined in SI-Fig. 7, recorded at 200 K. Overall, the spectra of the two crystalline preparations recorded at room temperature show very similar chemical shifts. Characteristic differences to the solution spectrum were observed[9] involving amino acids L8, V9, Y13, P20, R21, I30, T37, W41, V53, and Y57. These residues are located in crystal contact areas, with I30 and T37 shown in SI Fig. 8. Cross peaks involving the other threonine residues superimpose relatively well (SI-Figure 8 B, left spectrum). The largest difference between the spectra of the solution vs. the crystalline material appears for the C_δ chemical shift of I30 (Figure SI-Figure-8 A, right spectrum). The chemical shift patterns of I30 and T37 confirm that our samples consist largely of crystals.

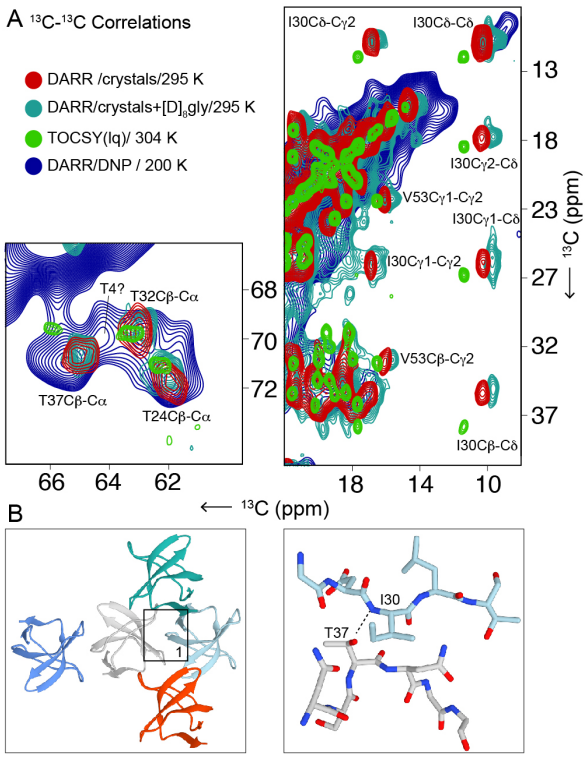

SI-Figure 8. : (A) Estimation of sample quality by solution and solid-state NMR, showing the regions with threonine C -C cross peaks (left) and with the signal pattern involving the C of I30 (right). Blue: DNP DONER spectrum with 20 mM CD_3-TOTAPOL-25 at 200 K, 25 ms mixing; red: solid state ^{13}C-^{13}C DARR spectrum of SH3 crystals at 295 K; Cyan: crystals with [D_8]-glycerol; green: solution state NMR ^{13}C-^{13}C 20 ms TOCSY (FLOPSY16) mixing at 304 K. (B) Orientation of protomers in the crystal structure 1U06 (left) and intermolecular contacts and possible hydrogen bond between I30 and T37 (right).

2.2 Acquisition of DNP MAS ssNMR spectra

All DNP MAS ssNMR spectra were recorded on a Bruker Avance III 9.4 T (400 MHz) wide-bore spectrometer system equipped with a 263 GHz gyrotron as a microwave source (~ 5 W and the end of the waveguide) and a triple resonance cryo-MAS probe. All samples were measured in standard 3.2 mm zirconia rotors, at spinning frequencies of 8000 ± 2 Hz for proline and 8889 ± 2 Hz for SH3 samples, respectively. Spectra were processed using Topspin 3.2.

Enhancements were determined by recording ^{13}C-CP spectra with and without microwave irradiation under otherwise identical conditions. For each temperature, the recycle delay was set to 1.3 x T_1. Proton decoupling (TPPM)[10] was set to 75 kHz and the acquisition time was 20 ms. For the CP, the ^{1}H and ^{13}C rf fields were set to 52 kHz and 44 kHz respectively, with a linear ramp from 75 % to 100 %. Off-spectra were recorded with 8 - 64 scans and on-spectra with 4 - 32 scans, depending on the signal intensities. 2-4 dummy scans were applied prior to acquisition. Enhancements

were determined by overlaying both spectra, scaling the off-spectrum to the size of the on-spectrum.

To achieve cryogenic temperatures a Bruker low-temperature MAS system was used. Sample temperatures were calibrated using both the KBr T_1 and chemical shifts values according to known procedure[11, 12.] The melting point of deuterated pentane was used as an internal standard for temperature calibration when using chemical shifts.

The temperatures of the bearing, VT and drive gases ('set temperatures') were equilibrated for at least 15 minutes before measurements. After turning the microwaves on or off, the temperatures of the samples were additionally equilibrated for at least 5 minutes. MW on and MW off spectra were recorded at the same temperature settings. All reported temperatures refer to calibrated temperatures with microwave irradiation (MW on), which are about 7 K higher than with MW off on our instrument. Proton T_1 values were measured using an inversion recovery sequence followed by a CP and detection on the carbon channel, employing delays of 10 μs, 0.1 s, 0.3 s, 1 s, 3 s, 10 s, 30 s and 60 s.

All two dimensional DNP MAS ssNMR ^{13}C-^{13}C- correlation spectra were typically recorded within 2.5 -3 hrs with a spectral width 388.1 x 496.6. For the spectra acquired at 200 K the direct evolution time 25 ms were used with 1948 points and 8 scans/ 4 dummy scans per row. In the indirect dimension 744 data points were recorded (States-TPPI). 4069 x 4069 data points were used to process the spectra with GM LB = -30 Hz; GB= 0.08 SSB = 3 in the direct and Qsine LB= 0.3 Hz; GB= 0.12; SSB = 2 in the indirect dimension.

Heteronuclear 2D NCACX/NCOCX experiments were recorded at 200 K using 8 steady scans, 32 dummy scans, 30 ms of DARR mixing and a relaxation delay of 2 s. For the CP $\omega_1C \sim 7/2\ \omega_r$, $\omega_1N \sim 9/2\ \omega_r$ for the NCACX and $\omega 1\ C \sim 11/2\ \omega_r$, $\omega_1N \sim 9/2\ \omega_r$ for the NCOCX CP periods with ~ 75 kHz decoupling was used. The direct dimension was acquired with 25 ms acquisition times and 1558 points (States TPPI) and 256 points (States TPPI) in the indirect dimension. The NCACX 3D experiments were recorded within 13 h, the NCOCX spectra in 9.5 h. For both spectra 4 steady

state scans and 32 dummy scans were used and acquired with 1558 in the direct and 64 and 88 points in the indirect dimension with 15 ms of DARR mixing. A spectral width of 388.2 on the direct carbon dimension, 73.01 on ^{15}N and 58.89 on the ^{13}C-CO dimensions was used. The spectra were processed with 4096x128x18 points.

2.3 MAS dependence of CD_3-TOTAPOL-25 vs ^{1}H-TOTAPOL

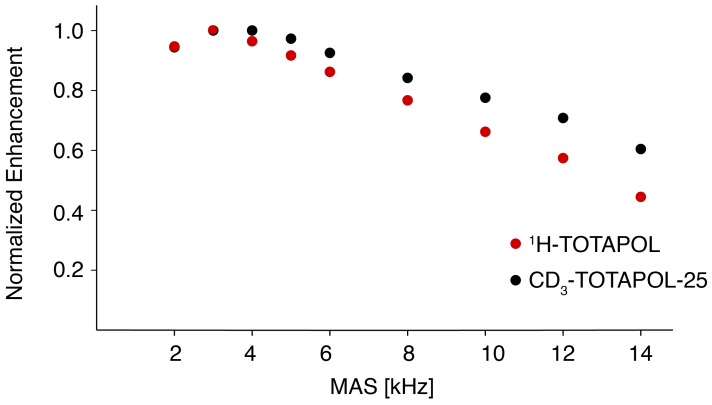

SI-Figure 9: MAS dependence at 110 K of ^{1}H DNP signal enhancement for ^{1}H-TOTAPOL and CD_3-TOTAPOL-25 measured at 263 GHz. All signal enhancements were measured via ^{13}C CP MAS experiment on 1 mg U-^{13}C-^{15}N proline with 20 mM biradical concentration (by weight) in GDH with and without microwave irradiation for each data point.

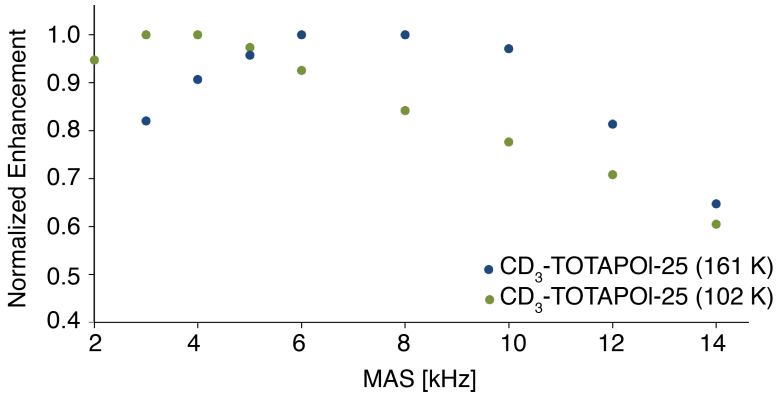

SI-Figure 10: Temperature dependence of ^{1}H enhancements for CD_3-TOTAPOL-25 measured at 263 GHz. All signal enhancements were measured via ^{13}C CP MAS experiment on 1 mg U-^{13}C-^{15}N proline with 20 mM biradical concentration (by weight) in GDH with and without microwave irradiation for each data point

2.4 2D NCACX spectrum

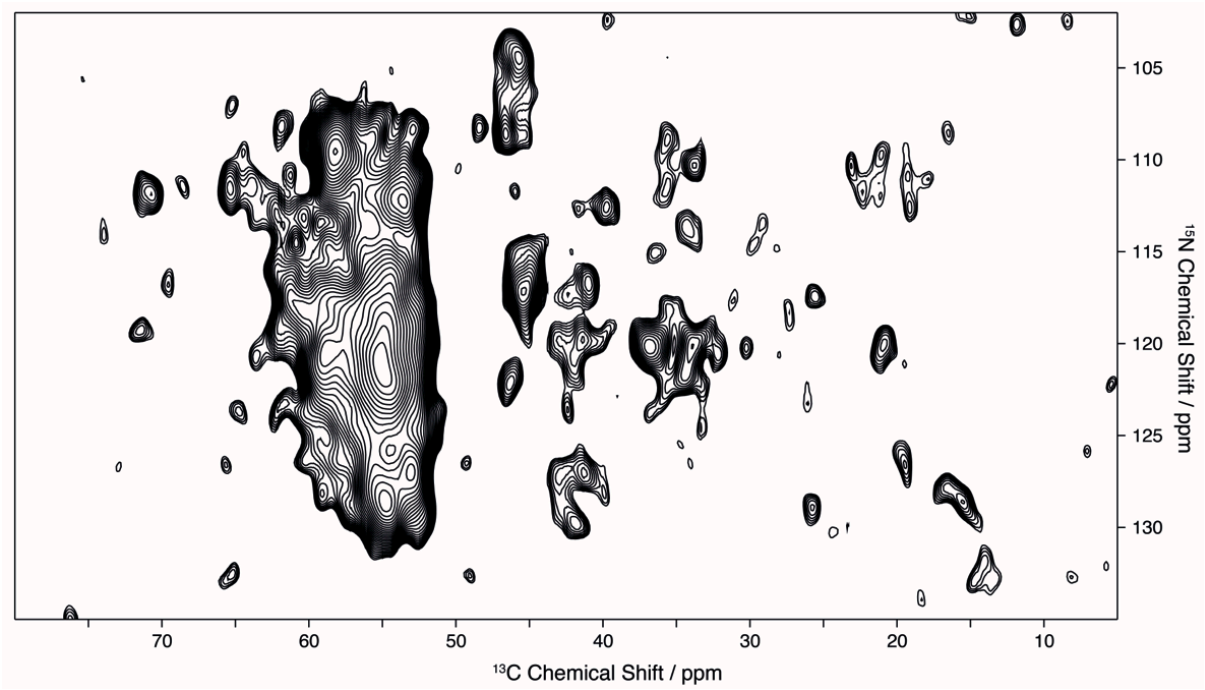

SI - Figure 11: 2D NCACX DNP enhanced ssMAS NMR spectra of microcrystalline α-spectrin SH3 protein containing 20 mM CD_3-TOTAPol-0 recorded at 200 K at a magnetic field strength of 9.4 T within 1 h at 8.8 kHz MAS spinning with 16 scans, 32 dummy scans a recycle delay of 0.7 sec 25 ms DARR mixing

3 EPR experiments

EPR experiments were performed on a home-built high-frequency pulsed EPR spectrometer[13, 14] at 180 GHz (G-band), corresponding to a static magnetic field of approximately 6.42 T for nitroxide radicals. Temperature control was achieved with an ITC 503 temperature control unit (Oxford Instruments). The applied microwave power was approximately 30 mW, with a π pulse length of about 85 ns to 90 ns, and a cylindrical resonator operating in the fundamental TE_{011} mode. To avoid saturation of the spectrometer receiver with high intensity echo signals, the frequency of the resonator was slightly detuned with respect to the spectrometer operation frequency to decrease the pulse flip angle. Samples were loaded into a silica capillary with an inner diameter of 0.40 mm. The electron spin longitudinal relaxation times T_{1e} were obtained from the saturation-recovery curves, as described in detail in the Supporting

Information to minimize contributions from spectral diffusion.[4] Measurements of the electron spin transversal relaxation time T_{2e} were performed with a two pulse Hahn echo sequence. Due to the fact that echo-decays were not mono-exponential, T_{2e} was represented by a time constant after which the echo decayed by a factor of *e*, where *e* is Euler's number

3.1 Pseudo continuous wave EPR spectra

Pseudo CW EPR spectra of TOTAPOL-1H and CD_3-TOTAPOL-25 obtained from Hahn echo-detected field-swept EPR spectra (see Fig. 3 in the main text) at different temperatures are depicted in **SI Figure 12**

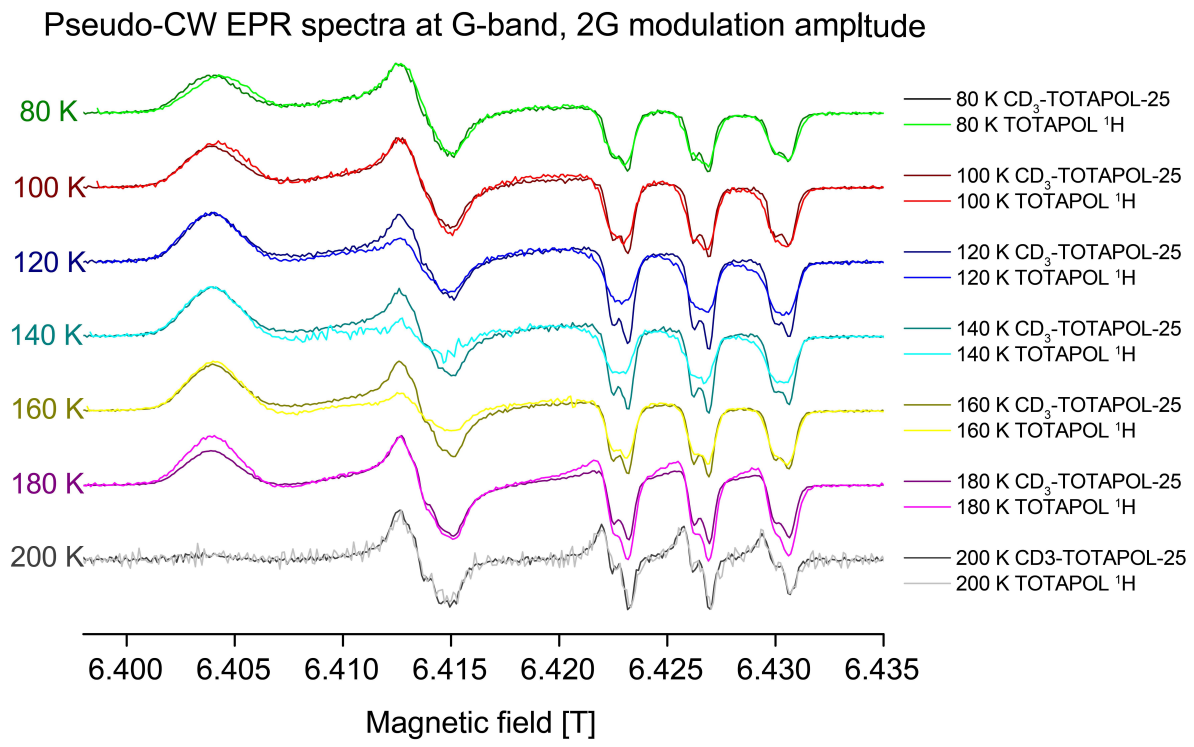

SI Figure 12. Pseudo CW G-band EPR spectra of TOTAPOL-^{1}H and CD_3-TOTAPOL-25 obtained at temperatures between 80 and 200 K. The spectra are normalized to the maximum value and vertically shifted for better visual comparison. The resonance fields were adjusted such that the spectral positions, corresponding roughly to g_{yy}, coincided for all spectra.

The pseudo CW EPR spectra are calculated with the function fieldmod in EasySpin[15] package for MATLAB with the pseudo-modulation amplitude of 2 G. As these EPR spectra obtained from the Hahn-echo detected field sweeps, the anisotropic

transversal relaxation rate contributes to the intensities of different regions of the spectrum as well. The splitting of about 19 MHz was observed in the g_{zz} region of the spectra, that is better resolved for CD_3-TOTAPOL-25 sample. This value is similar to the intra-molecular electron-electron dipolar coupling for TOTAPOL radical of about 22-23 MHz.[2]

3.2 Electron spin longitudinal relaxation times measurements

For electron spin longitudinal relaxation time (T_{1e}) measurements a saturation-recovery experiment (**SI Figure 13**) was used. As saturation, a pulse-train, consisting of 64 pulses with the length corresponding roughly to π/2 pulse with the inter-pulse delay time of approximately $2T_{2e}$ to $3T_{2e}$, was applied. T_{2e} is the electron spin transversal relaxation time (see section 3) at corresponding field position. The detection sequence applied after delay time T was a two-pulse Hahn-echo sequence. The delay time T was incremented to record the experimental curves

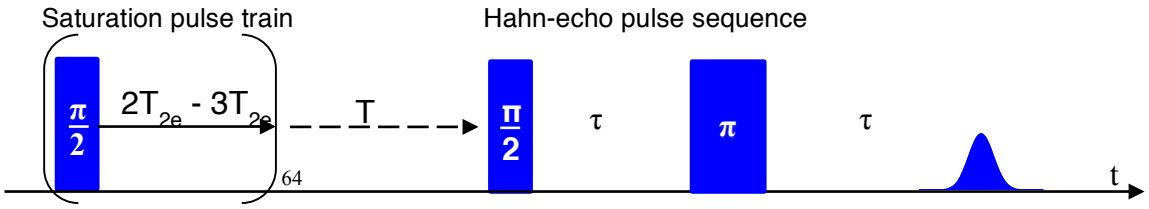

SI Figure 13: Saturation-recovery pulse sequence used for T_{1e} measurements on G-band EPR spectrometer

The experimental saturation recovery curves of TOTAPOL-^{1}H and CD_3-TOTAPOL-25 are depicted in **SI Figure 14**.

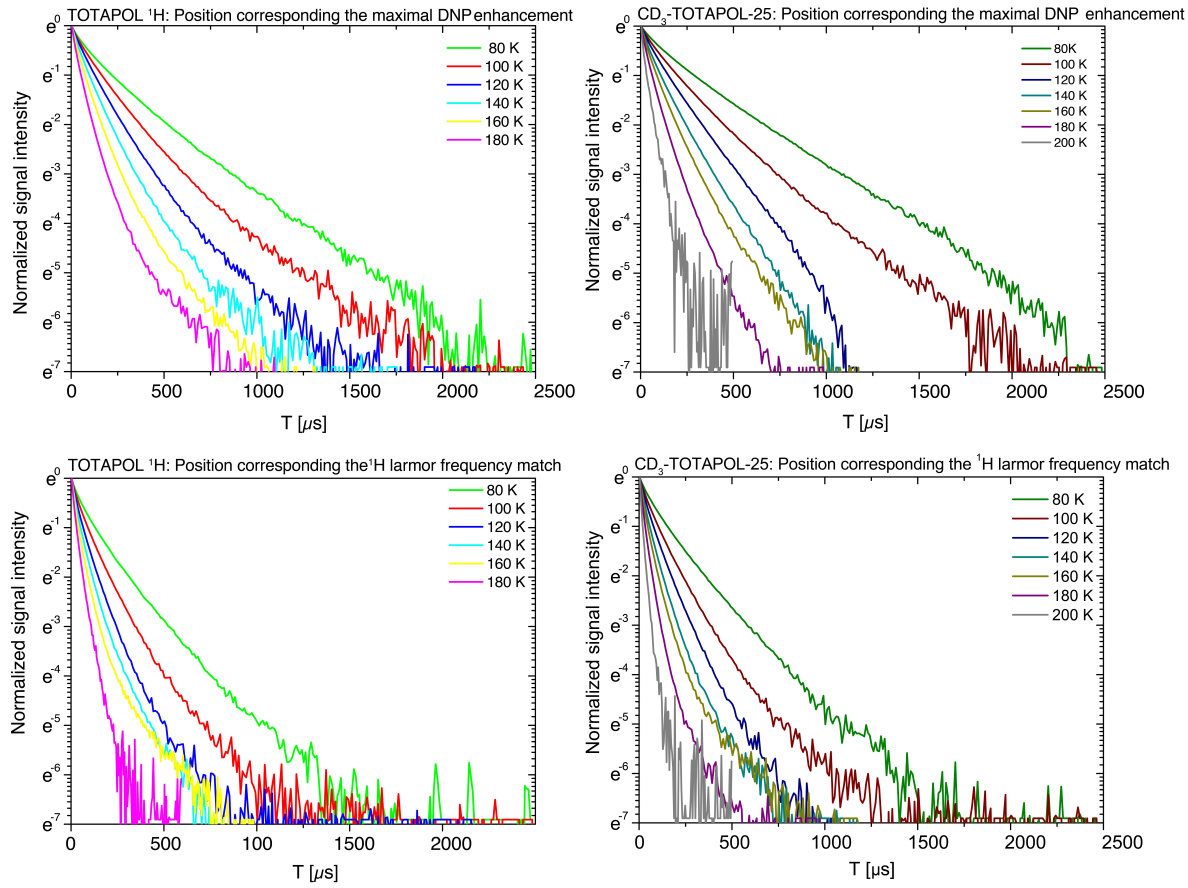

SI Figure 14. Experimental saturation-recovery curves of TOTAPOL-^{1}H (left side) and CD_3-TOTAPOL-25 (right side). **Upper row**: saturation recovery curves were obtained at the spectral position 2 (see Figure 3, the main text). **Bottom row**: saturation recovery curves were obtained at the spectral position 1

The experimental saturation-recovery curves are represented (**SI Figure 14**) using the following procedure. The constant offset $I(T\rightarrow\infty)$, which corresponds to the echo intensity at the time T exceeding $5T_1$, was subtracted from the experimental saturation-recovery curves. The obtained curves were then inverted and normalized, such that the intensity ranged from 1 at the initial time of $T = T_0$ till 0 at the time of $T\rightarrow\infty$. The logarithmic scale was applied for the axes of ordinates in order to have a better visualization for the character of the decay. All the curves are not a mono-exponential. At least two components with different decay constants and different weights are presented. One of the components (shorter decay constant) is strongly affected by spectral diffusion due to non-ideal saturation during the saturation pulse train. Therefore, the following procedure for extracting the longitudinal relaxation time was chosen.[4] The time constants τ_1, τ_2 and τ_3 after which the echo decayed by a factor of e, e^2 and e^3, respectively, were determined. The decay between τ_2 and τ_3

contains much less contribution from spectral diffusion and, hence, more reliably represents the T_{1e} time, though this part of the curves contains certain degree of noise. The values are given in **SI Table 1** (the 4th column).

Table 1. Longitudinal relaxation times.

TOTAPOL 1H: Position 2					
Temperature, K	τ_2, μs	τ_3, μs	**$T_{1e} \approx \tau_3 - \tau_2$, μs**	T_{fast}, μs	**T_{slow}, μs**
80	519	865	**346**	76	**321**
100	372	613	**241**	72	**231**
120	280	452	**172**	69	**179**
140	215	349	**134**	51	**137**
160	165	272	**107**	40	**110**
180	118	194	**76**	28	**80**
TOTAPOL 1H: Position 1					
Temperature, K	τ_2, μs	τ_3, μs	**$T_{1e} \approx \tau_3 - \tau_2$, μs**	T_{fast}, μs	**T_{slow}, μs**
80	314	526	**212**	48	**202**
100	209	345	**136**	40	**137**
120	147	245	**98**	32	**99**
140	116	195	**80**	27	**82**
160	91	155	**64**	23	**70**
180	65	109	**44**	15	**44**
CD_3-TOTAPOL-25: Position 2					
Temperature, K	τ_2, μs	τ_3, μs	**$T_{1e} \approx \tau_3 - \tau_2$, μs**	T_{fast}, μs	**T_{slow}, μs**
80	670	1083	**413**	99	**401**
100	451	733	**282**	81	**274**
120	333	532	**199**	52	**192**
140	245	396	**151**	44	**147**
160	196	321	**125**	37	**121**
180	137	222	**85**	28	**84**
200	77	124	**47**	11	**46**
CD_3-TOTAPOL-25: Position 1					
Temperature, K	τ_2, μs	τ_3, μs	**$T_{1e} \approx \tau_3 - \tau_2$, μs**	T_{fast}, μs	**T_{slow}, μs**
80	356	581	**225**	61	**222**
100	234	384	**150**	44	**148**
120	174	285	**111**	33	**107**
140	128	210	**82**	27	**83**
160	103	175	**72**	25	**73**
180	72	117	**45**	17	**49**
200	42	69	**27**	8	**27**

The data are the values, obtained from the experiment or their fits, rounded to the nearest integer numbers

The dependence of the longitudinal relaxation time $T_{1e} \approx \tau_3 - \tau_2$ on temperature is depicted in **SI Figure 15**.

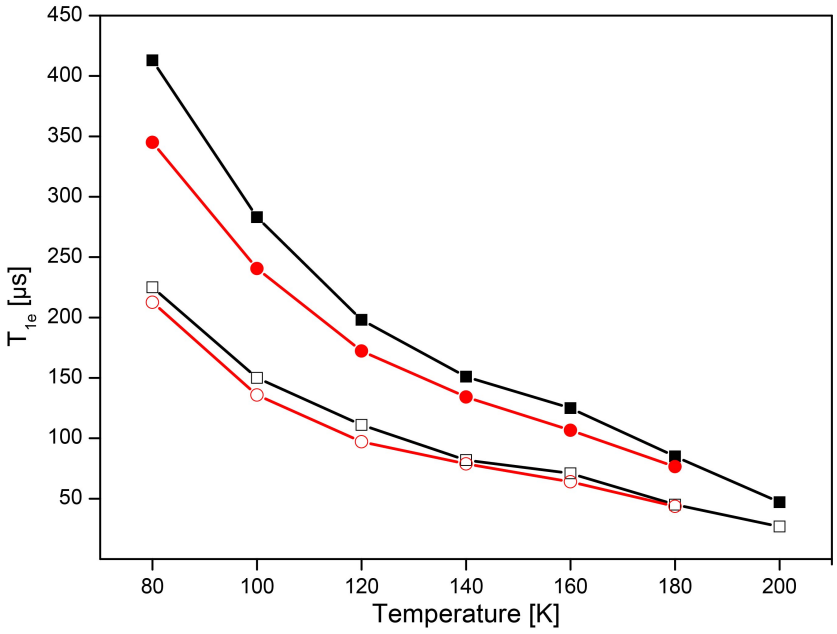

SI Figure 15. Longitudinal relaxation time T_{1e} dependence on temperature for TOTAPOL-^{1}H (red) and CD_3-TOTAPOL-25 (black) obtained at two spectral positions. The filled symbols represent the spectral position 2 and the unfilled symbols represent the spectral position 1 (See Figure 3, the main text).

Alternatively, T_{1e} times were obtained from the fits of the experimental saturation recovery curves with the bi-exponential function (Formula 1):

$$S(T) = A_1\left(1 - \exp\left(-\frac{T}{T_{slow}}\right)\right) + A_2\left(1 - \exp\left(-\frac{T}{T_{fast}}\right)\right) + C \qquad (1)$$

where S(T) is the signal intensity at given delay time T, A_1 and A_2 represent the weights of the components, decaying with slow (T_{slow}) and fast (T_{fast}) time constants, respectively, and constant C represents the residual magnetization at the time of $T = T_0$. The spectral diffusion, mimicked in the saturation-recovery curves as a component decaying with a constant T_{fast}, and the residual magnetization, are both occur due to non-ideal saturation during the pulse train. Both, T_{fast} and T_{slow} decay constants are given in **SI Table 1** (the 5th and 6th column, respectively). The decay constant T_{slow} represents the T_{1e}. The values for T_{1e} obtained with both strategies are similar. However, as the longitudinal relaxation times obtained as $T_{1e} \approx \tau_3 - \tau_2$ do not rely on the fitting procedure, including a variation of five parameters, the uncertainty

of obtaining the data with this procedure is reduced. Therefore, these data are further used.

3.3 Electron spin transversal relaxation time measurements

A two pulse Hahn-echo sequence depicted in SI Figure 16 was used for the measurements of the transversal relaxation time.

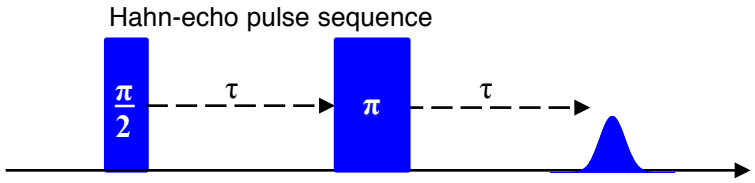

SI Figure 16. Hahn-echo pulse sequence used for T_{2e} measurements

The inter-pulse delay time τ was incremented from 200 ns in order to record the decay of the echo signal amplitude. The normalized Hahn-echo decay curves are depicted in **SI Figure 17** in the logarithmic scale applied to the axes of ordinates. As the echo intensity decays are not mono-exponential functions, the transversal relaxation time was mimicked by the phase memory time (T_{me}), obtained as a time constant T_{2e} after which the echo decayed by a factor of *e*.

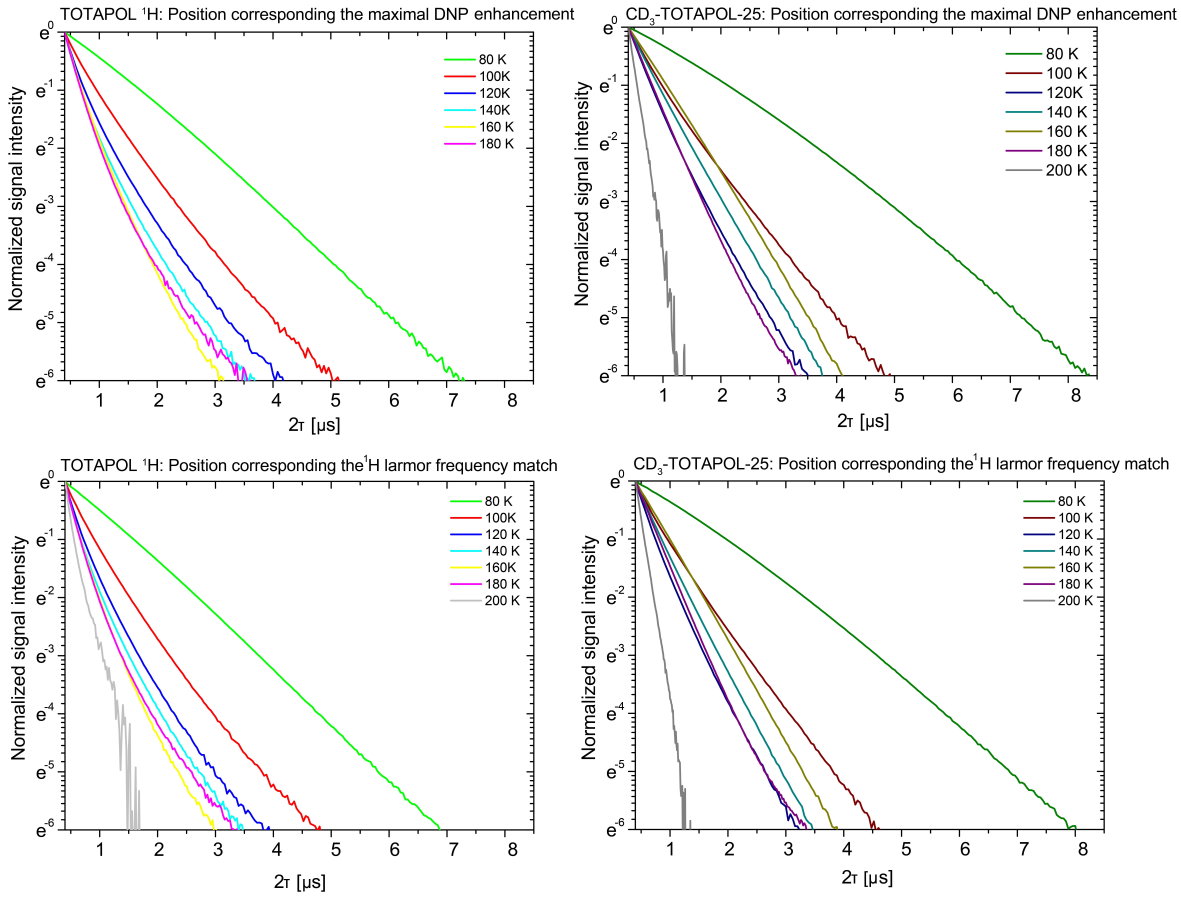

SI Figure 17. Experimental Hahn-echo decay curves of TOTAPOL 1H (left side) and CD_3-TOTAPOL-25 (right side). **Upper row**: saturation recovery curves were obtained at the spectral position 2 (see Figure 3, the main text). **Bottom row**: saturation recovery curves were obtained at the spectral position 1

The values for the transversal relaxation time are depicted in **SI Table 2** together with corresponding T_{1e} and a product of T_{1e}·T_{2e}, which representing the electron spins saturation factor.

SI Table 2. The transversal relaxation time with corresponding longitudinal relaxation time and saturation factor $T_{1e}{\cdot}T_{2e}$

TOTAPOL 1H: Position 2			
Temperature, K	$T_{1e}{\approx}\tau_3 - \tau_2$, μs	T_{2e}, μs	$T_{1e}{\cdot}T_{2e}$, μs^2
80	346	1.31	453
100	241	0.55	133
120	172	0.35	60
140	134	0.29	39
160	107	0.30	32
180	76	0.28	21
TOTAPOL 1H: Position 1			
Temperature, K	$T_{1e}{\approx}\tau_3 - \tau_2$, μs	T_{2e}, μs	$T_{1e}{\cdot}T_{2e}$, μs^2
80	212	1.19	252
100	136	0.51	69
120	98	0.32	31
140	80	0.27	22
160	64	0.27	17
180	44	0.26	11
200	-	0.15	-
CD_3-TOTAPOL-25: Position 2			
Temperature, K	$T_{1e}{\approx}\tau_3 - \tau_2$, μs	T_{2e}, μs	$T_{1e}{\cdot}T_{2e}$, μs^2
80	413	1.72	710
100	282	0.58	164
120	199	0.40	80
140	151	0.52	79
160	125	0.66	83
180	85	0.41	35
200	47	0.15	7
CD_3-TOTAPOL 25: Position 1			
Temperature, K	$T_{1e}{\approx}\tau_3 - \tau_2$, μs	T_{2e}, μs	$T_{1e}{\cdot}T_{2e}$, μs^2
80	225	1.57	353
100	150	0.55	83
120	111	0.35	39
140	82	0.45	36
160	72	0.60	43
180	45	0.41	18
200	27	0.15	4

The data corresponding the T_{2e} are presented as rounded to the nearest second decimal digit

The transversal relaxation time dependences on temperature are depicted in **SI Figure 18**.

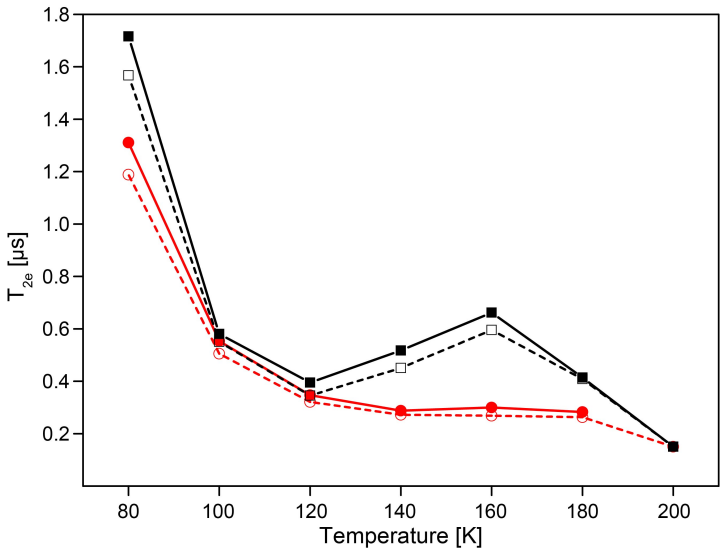

SI Figure 18. Transversal relaxation time dependence on temperature for TOTAPOL-^{1}H (red) and CD_3-TOTAPOL-25 (black) obtained at two spectral positions. The filled symbols with solid lines represent the spectral position 2 and the unfilled symbols with dashed lines represent the spectral position 1 (See Figure 3, the main text)

The dependences of product of $T_{1e}{\cdot}T_{2e}$ on temperature are depicted in **SI Figure 19**.

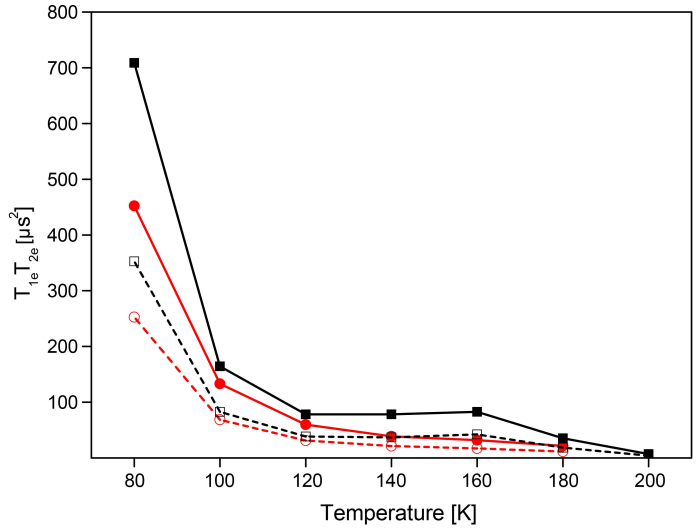

SI Figure 19. Temperature dependence of product of $T_{1e}{\cdot}T_{2e}$ for TOTAPOL-^{1}H (red) and CD_3-TOTAPOL-25 (black) obtained at two spectral positions. The filled symbols with solid lines represent the spectral position 2 and the unfilled symbols with dashed lines represent the spectral position 1 (See Figure 3, the main text).

References

1. H. E. Gottlieb, V. Kotlyar and A. Nudelman, *The Journal of Organic Chemistry*, 1997, **62**, 7512-7515.
2. C. Song, K.-N. Hu, C.-G. Joo, T. M. Swager and R. G. Griffin, *Journal of the American Chemical Society*, 2006, **128**, 11385-11390.
3. E. G. Rozantsev and H. Ulrich, *Free nitroxyl radicals*, Plenum press, New York; London, 1970.
4. R. Chiarelli and A. Rassat, *Tetrahedron*, 1973, **29**, 3639-3647.
5. F. Barbarin, B. Chevarin, J. P. Germain, C. Fabre and D. Cabaret, *Molecular Crystals and Liquid Crystals*, 1978, **46**, 195-207.
6. K.-i. Yamada, Y. Kinoshita, T. Yamasaki, H. Sadasue, F. Mito, M. Nagai, S. Matsumoto, M. Aso, H. Suemune, K. Sakai and H. Utsumi, *Archiv der Pharmazie*, 2008, **341**, 548-553.
7. P. Schattling, F. D. Jochum and P. Theato, *Chemical Communications*, 2011, **47**, 8859-8861.
8. S. R. Burks, J. Bakhshai, M. A. Makowsky, S. Muralidharan, P. Tsai, G. M. Rosen and J. P. Kao, *J Org Chem*, 2010, **75**, 6463-6467.
9. J. Pauli, M. Baldus, B. van Rossum, H. de Groot and H. Oschkinat, *ChemBioChem*, 2001, **2**, 272-281.
10. A. E. Bennett, C. M. Rienstra, M. Auger, K. V. Lakshmi and R. G. Griffin, *The Journal of chemical physics*, 1995, **103**, 6951-6958.
11. K. R. Thurber and R. Tycko, *Journal of magnetic resonance*, 2009, **196**, 84-87.
12. K. R. Thurber, W. M. Yau and R. Tycko, *Journal of magnetic resonance*, 2010, **204**, 303-313.
13. M. Rohrer, O. Brügmann, B. Kinzer and T. F. Prisner, *Applied magnetic resonance*, 2001, **21**, 257-274.
14. V. P. Denysenkov, T. F. Prisner, J. Stubbe and M. Bennati, *Applied magnetic resonance*, 2005, **29**, 375-384.
15. S. Stoll and A. Schweiger, *Journal of magnetic resonance*, 2006, **178**, 42-55.